



Numerical Simulation of Time-Dependent Viscous Fluid Flow with Upward and Downward Fluctuation of Spinning Disk

Samia Bushnaq, Asif Ullah Hayat and Hassan Khan

ABSTRACT: This research used a parametric approach to assess fluid flow across a gyrating disk under magnetic fields and heat propagation processes. The governing equations, including Navier-Stokes, energy, concentration, and Maxwell equations, were appropriately represented as a system of non-linear ODEs. Numerical procedures, including the Parametric Continuation Method (PCM), were used to solve the equations, and the findings were compared to another numerical Matlab scheme boundary value solver for scale reliability purposes. Results, including the impact of convective boundary conditions, suction, and wall injection, were presented in tabular and graphical forms. The spinning disk's motion led to comparable findings in an injection scenario and contributed to wall suction-like effects during downhill motion.

Key Words: Parametric Continuation Method (PCM), Maxwell equation, fluctuating disk, spinning disk, Dufour and Soret number.

Contents

1 Introduction	1
2 Mathematical Formulation	3
3 Problem Solution	5
4 Result and Discussion	7
5 Conclusion	11

1. Introduction

Heat and mass transference across a rotating disc is used in a variety of heat exchangers and electrical equipment. Computer hardware for storage, thermal energy-producing systems, gas turbines, spinning devices, geothermal industries, and many types of medical instruments are some of the uses of such problems [1]. Fluid flow over a spinning disc is extremely significant since it is used in a wide range of businesses, engineering, and scientific disciplines. Hafeez et al. [2] evaluated the magnetized flow of an Oldroyd-B fluid across a revolving disc by employing the modified Fourier's law rather than the standard Fourier's law. It has been discovered that when the relaxation time factor is increased, the fluid velocity tends to decrease. Ahmadian et al. [3] addressed a 3D numerical analysis of an unstable nano liquid flow with variable thermal conductivity produced by the upward/downward movement of a wavy rotating disc. When associated to a flat superficial, the wavy revolving surface improves heat transference by up to 15%. Khan et al. [4] used a non-linear radiative viscous fluid flow with slip conditions and mixed convection across a stretchable spinning disc to investigate the influence of entropy production. Using the Matlab algorithm boundary value solver (bvp4c) and a porous spinning disc, Li et al. [5] developed fractional assessments for nano fluid flow with temperature and mass slip parameters. Zhou et al. [6] developed a Maxwell fluid model utilizing Buongiorno's formulation over a permeable turning disc with a constant suction and injection impact. The mass propagation accelerates considerably as the thermophoresis factor is enhanced, whereas radial and angular velocities reduce as the viscosity coefficient is elevated. Tassaddiq et al. [7] designed an innumerable permeable spinning disc with an incompressible nano fluid flow. Their goal was to improve our knowledge of energy depletion in industrial and technical settings. The combination of CNTs and Fe₃O₄ nano fluids significantly improves the mass and thermal energy diffusion rate, according to the findings.

Maxwell's equations are indeed a sequence of correlated PDEs that constitute the basis of classical conventional optics and electromagnetism, together with the Lorentz force law. The equations serve as a mathematical formula for optical, electric, and radio technology including power production, electric motors, lenses, wireless communication, and radar, etc. They explain how currents, charges, and field changes create magnetic and electric fields. The algorithms are renamed because James Clerk Maxwell, a mathematician, and physicist, reported an early version of the equations in 1861, which contained the Lorentz force law. A innovative theory of instability is presented, based on the similarities between turbulent hydrodynamics and electromagnetism, to characterize the dynamic characteristics of fluid flow [8]. Euler's equation of motion, as well as the equations of continuity, vorticity, and entropy, control the motion of a compressible ideal fluid. This system may be recast to resemble electromagnetism, which is controlled by Maxwell's equations with source terms. Fluid mechanics examples are used to illustrate the importance of reformulation [9]. Luo et al. [10] and Yao et al. [11] addressed the massive asymptotic behavior of the solutions of the Maxwell equations coupled with Navier–Stokes equations for the weak deformation wave under tiny perturbations of starting data and a small dielectric constant. The conclusion is based on basic L2 energy techniques. Ahmadian et al. [12] examined the dynamics of Maxwell nanofluid flow by computing the Maxwell equations along with the 3D Navier–Stokes equations across two gyrating discs. According to the findings, the disc stretching action opposes the flow behavior. Zhang [13] has interpreted the Navier–Stokes–incompressible Maxwell's system with the Ohm law, which may be obtained from the Navier–Stokes–Maxwell two-fluid system, when the momentum transition constant reaches zero. The technique is based on the electric and magnetic field's decaying and dissipating characteristics.

Complex nonlinear boundary value issues that are difficult to solve are common in the professional disciplines. For numerous issues that are typically handled by other quantitative techniques, progress is sensitive to the relaxation variables and initial approach. The PCM's purpose is to investigate the technique's generalization as a viable nonlinear problem solution [14]. The 3D unsteady fluid and energy conduction through the surface of a semi extensible spinning disc was highlighted by Shuaib et al. [15]. The fluid has been studied in the presence of a magnetic field from the outside. Shuaib et al. [16] found the phenomenon of an ionic transitioning boundary layer flow across a swaying disc. The ionic compositions were calculated using the Poisson's, Lorentz, and Navier–Stokes equations. Wang et al. [17] used a parametric continuation approach to offer consistency assessment of complex equations for engineering purposes. They also focused on static bifurcation, which occurs while solving nonlinear starting value problems with distinct characteristic roots, and developed a method for estimating the bifurcation points quickly.

Keeping in view the above literature and its application in different sectors, we have modeled time-dependent viscous fluid flow across a gyrating disk with upward and downward movement. The major goal of this research is to study the fluid flow under the influence of magnetic fields and heat propagation characteristics. The governing equations consisting of traditional Navier–Stokes equation and Maxwell equations have been studied. The governing equations are condensed to the system of non-linear ODEs through the similarity approach. The acquired system of differential equations has been dealt via numerical procedure (PCM). For reliability and validity purposes of the scheme, the outcomes are compared to bvp4c. The numerical findings are provided in tabular and graphical forms. The next section explains the mathematical formulation and solution framework.

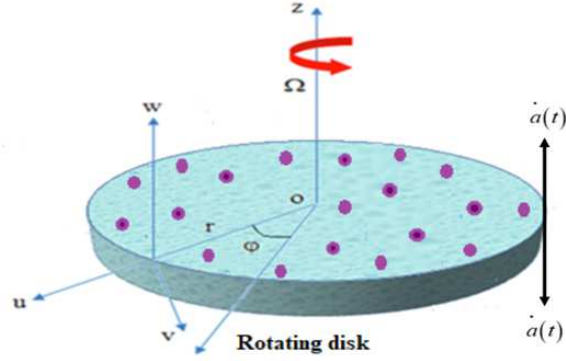


Figure 1: Fluid flow over a spinning disk

2. Mathematical Formulation

An unsteady, incompressible Newtonian fluid flow with up and downward fluctuation generated due to spinning of the permeable infinite disk is examined. Figure 1 displays the flow mechanism due to the up and downward movement of gyrating disk. The disk moves around the z -axis with $\Omega(t)$ (angular velocity) is dependent on time. Initially, when $t = 0$, the disk is at $a(0) = h$, but then with some time t the disk moves with vertical velocity $w = a(t)$ to the position $z = a(t)$. The dissipation of viscous energy in a fluid flow is ignored and because an axisymmetric flow condition is assumed, derivatives along the perpendicular direction have been ignored. The interface of a heated fluid heated the disc surface having concentration and temperature (C_f & T_f). While, far away from the surface of the disc the ambient concentration and temperature are (C_∞ & T_∞). The modeled equations are rebound as [12,13,14,15,16,17,18,19,20]:

$$\frac{\partial u}{\partial r} + \frac{\partial w}{\partial z} + \frac{u}{r} = 0, \quad (2.1)$$

$$\frac{\partial u}{\partial t} + u \frac{\partial u}{\partial r} + w \frac{\partial u}{\partial z} - \frac{v^2}{r} = -\frac{1}{\rho} \frac{\partial p}{\partial r} + v \left(\frac{\partial^2 u}{\partial r^2} + \frac{\partial^2 u}{\partial z^2} + \frac{1}{r} \frac{\partial u}{\partial r} - \frac{u}{r^2} \right), \quad (2.2)$$

$$\frac{\partial v}{\partial t} + u \frac{\partial v}{\partial r} + w \frac{\partial v}{\partial z} + \frac{vu}{r} = v \left(\frac{\partial^2 v}{\partial r^2} + \frac{\partial^2 v}{\partial z^2} + \frac{1}{r} \frac{\partial v}{\partial r} - \frac{v}{r^2} \right), \quad (2.3)$$

$$\frac{\partial w}{\partial t} + u \frac{\partial w}{\partial r} + w \frac{\partial w}{\partial z} = -\frac{1}{\rho} \frac{\partial p}{\partial z} + v \left(\frac{\partial^2 w}{\partial r^2} + \frac{\partial^2 w}{\partial z^2} + \frac{1}{r} \frac{\partial w}{\partial r} \right), \quad (2.4)$$

$$\frac{\partial T}{\partial t} + u \frac{\partial T}{\partial r} + w \frac{\partial T}{\partial z} = \frac{k}{\rho c_p} \left(\frac{\partial^2 T}{\partial r^2} + \frac{1}{r} \frac{\partial T}{\partial r} + \frac{\partial^2 T}{\partial z^2} \right) + \frac{Dk_T}{c_z c_p} \left(\frac{\partial^2 C}{\partial r^2} + \frac{1}{r} \frac{\partial C}{\partial r} + \frac{\partial^2 C}{\partial z^2} \right), \quad (2.5)$$

$$\frac{\partial C}{\partial t} + u \frac{\partial C}{\partial r} + w \frac{\partial C}{\partial z} = D \left(\frac{\partial^2 C}{\partial r^2} + \frac{1}{r} \frac{\partial C}{\partial r} + \frac{\partial^2 C}{\partial z^2} \right) + \frac{Dk_T}{T_m} \left(\frac{\partial^2 T}{\partial r^2} + \frac{1}{r} \frac{\partial T}{\partial r} + \frac{\partial^2 T}{\partial z^2} \right), \quad (2.6)$$

$$\frac{\partial B_r}{\partial t} = -w \frac{\partial B_r}{\partial z} - Br \frac{\partial B_w}{\partial z} + u \frac{\partial B_z}{\partial z} + \frac{1}{\sigma \mu} \left(\frac{\partial^2 B_r}{\partial r^2} + \frac{\partial^2 B_r}{\partial z^2} + \frac{1}{r} \frac{\partial B_r}{\partial r} - \frac{Br}{r^2} \right), \quad (2.7)$$

$$\frac{\partial B_z}{\partial t} = w \frac{\partial B_r}{\partial r} + Br \frac{\partial B_w}{\partial r} + \frac{1}{r} w Br - u \frac{\partial B_z}{\partial r} - Bz \frac{\partial u}{\partial r} - \frac{1}{r} u Bz + \frac{1}{\sigma \mu} \left(\frac{\partial^2 B_z}{\partial r^2} + \frac{\partial^2 B_z}{\partial z^2} + \frac{1}{r} \frac{\partial B_z}{\partial r} \right) \quad (2.8)$$

Where, C , T , T_m , c_z , k_T , D , c_P , k , v , μ , p , ρ represent concentration, temperature, fluid mean temperature, concentration susceptibility, thermal diffusion ratio, mass diffusivity, specific heat, thermal conductivity, kinetic viscosity, dynamic viscosity, pressure, and fluid density respectively.

The boundary conditions are:

$$\begin{cases} u = 0, v = r\Omega, w = \beta a(t), -k\left(\frac{\partial T}{\partial z}\right) = h_1(T_f - T), -D\left(\frac{\partial C}{\partial z}\right) = h_2(C_f - C), \\ Br = Bz = 0 \text{ at } z = a(t), \\ u \rightarrow 0, v \rightarrow 0, w \rightarrow 0, T \rightarrow T_\infty, C \rightarrow C_\infty, Br = \frac{dM_0}{2R}, Bz = -\alpha M_0 \text{ as } z \rightarrow \infty \end{cases} \quad (2.9)$$

Where, β is the surface permeability, in which $\beta = 1$ show disk surface impermeability, $\beta > 1$ injection and $\beta < 1$ suction effect of the disk surface. Furthermore, h_1 and h_2 are the constant heat and mass transition.

$$\begin{cases} u = \frac{rv}{a(t)}f(\eta), v = \frac{rv}{a(t)}g(\eta), w = \frac{v}{a(t)}h(\eta), \\ p = \frac{pv^2}{a(t)}P(\eta), Br = \frac{r\Omega M_0}{a(t)}m'(\eta), Bz = \frac{M_0(2v_f\Omega)^{0.5}}{a(t)}n(\eta), \\ C = C_\infty + (C_w - C_\infty)\varphi(\eta), T = T_\infty + (T_w - T_\infty)\theta(\eta), \eta = \frac{Z}{a(t)} - 1 \end{cases} \quad (2.10)$$

We derive the preceding series of ODEs by using Eq. (2.10) in Eqs. (2.1-2.8):

$$2f + h' = 0, \quad (2.11)$$

$$f'' - hf' - f^2 + g^2 + S\left(\frac{\eta+1}{2}f' + f\right) = 0, \quad (2.12)$$

$$g'' - hg' - 2fg + S\left(\frac{\eta+1}{2}g' + g\right) = 0, \quad (2.13)$$

$$h'' - hh' + S\left(\frac{\eta+1}{2}h' + \frac{h}{2}\right) = 0, \quad (2.14)$$

$$\theta'' - Prh\theta' + PrS\left(\frac{\eta+1}{2}\theta'\right) + PrDu\theta'' = 0, \quad (2.15)$$

$$\varphi'' - Sch\varphi' + ScS\left(\frac{\eta+1}{2}\varphi'\right) + ScSr\theta'' = 0, \quad (2.16)$$

$$m''' - Bt\left(-hm'' + m'h' + fn' + nf' + S\left(\frac{m''\eta}{2} + m'\right)\right) = 0, \quad (2.17)$$

$$n'' = -Bt\left(2hm' + 2nf - \frac{S}{2}(n'\eta + n)\right), \quad (2.18)$$

The transform condition:

$$\begin{cases} f(0) = 0, g(0) = \omega, h(0) = \frac{\beta S}{2}, \theta'(0) = -\beta_1(1 - \theta(0)), \varphi'(0) = -\beta_2(1 - \varphi(0)), \\ m'(\eta) \rightarrow 0, n(\eta) \rightarrow 0 \text{ as } \eta = 0 \\ f(\infty) \rightarrow 0, g(\infty) \rightarrow 0, h(\eta) \rightarrow 0, \theta(\infty) \rightarrow 0, \varphi(\infty) \rightarrow 0, m'(\eta) \rightarrow 0, \text{ as } \eta = \infty \end{cases} \quad (2.19)$$

The dimensionless parameters and number are expressed as [18]:

Here, $Pr = \frac{\mu c_p}{k}$ is the Prandtl number, $S = \frac{2a\dot{a}}{v}$ is the disk contracting and expanding factor, $Du = \frac{DT_k}{vc_s c_p}$ is the Dufour number, $Sr = \frac{DT_k}{vT_m}$ is the Soret number, $\beta_1 = \frac{h_1 a}{k}$ is the mass transition Biot number, $\beta_2 = \frac{h_2 a}{D}$ is the mass transition Biot number, $\Gamma = \frac{\Omega a^2}{v}$ is the disk rotation term, and $Sc = \frac{v}{D}$ is the Schmidt number.

3. Problem Solution

The following steps demonstrate the fundamental notion of applying the (PCM) technique to a system of ODEs (2.11-2.18) with their boundary conditions (2.19):

Step 1: Converting the BVP system to a first-order ODE system.

In order to do this, the following functions will be introduced.

$$\begin{cases} f = \zeta_1, & f' = \zeta_2, & g = \zeta_3, & g' = \zeta_4, & h = \zeta_5, & h' = \zeta_6, & \theta = \zeta_7, & \theta' = \zeta_8, \\ \varphi = \zeta_9, & \varphi' = \zeta_{10}, & m = \zeta_{11}, & m' = \zeta_{12}, & m'' = \zeta_{13}, & n = \zeta_{14}, & n' = \zeta_{15} \end{cases} \quad (3.1)$$

Using transformation (3.1) into the BVP (2.11- 2.19), which have the following form:

$$2\zeta_1 + \zeta_6 = 0, \quad (3.2)$$

$$\zeta_2 + (S\frac{\eta+1}{2} - \zeta_5 f)\zeta_2 - \zeta_1^2 + \zeta_3^2 + S\zeta_1 = 0, \quad (3.3)$$

$$\zeta_4 + (S\frac{\eta+1}{2} - \zeta_5)\zeta_4 - 2\zeta_1\zeta_3 + S\zeta_3 = 0, \quad (3.4)$$

$$\zeta_6 - (\zeta_5 - S\frac{\eta+1}{2})\zeta_6 + \frac{S\zeta_5}{2} = 0, \quad (3.5)$$

$$\zeta_8 + (PrS(\frac{\eta+1}{2}) - Pr\zeta_5)\zeta_8 + PrDu\zeta'_{10} = 0, \quad (3.6)$$

$$\zeta'_{10} - (Sch - ScS(\frac{\eta+1}{2}))\zeta_{10} + ScSr\zeta'_8 = 0, \quad (3.7)$$

$$\zeta'_{13} - Bt((S\frac{\eta}{2} - \zeta_5)\zeta_{13} + \zeta_{12}\zeta_6 + \zeta_1\zeta_6 + \zeta_5\zeta_2 + S\zeta_{12}) = 0, \quad (3.8)$$

$$\zeta'_{15} + Bt(2\zeta_5\zeta_{12} + 2\zeta_{14}\zeta_1 - \frac{S}{2}(\zeta_{15}\eta + \zeta_{15})) = 0, \quad (3.9)$$

with the corresponding boundary conditions.

$$\begin{cases} \zeta_1(0) = 0, & \zeta_3(0) = \omega, & \zeta_5(0) = \beta\frac{S}{2}, & \zeta_8(0) = -\beta_1(1 - \zeta_7(0)), & \zeta_{10}(0) = -\beta_2(1 - \zeta_9(0)), \\ \zeta_{12}(\eta) \rightarrow 0, & \zeta_{14}(\eta) \rightarrow 0 & \text{at } \eta = 0, \\ \zeta_1(\infty) \rightarrow 0, & \zeta_3(\infty) \rightarrow 0, & \zeta_5(\infty) \rightarrow 0, & \zeta_7(\infty) \rightarrow 0, & \zeta_9(\infty) \rightarrow 0, & \zeta_{12}(\eta) \rightarrow 0, & \zeta_{14}(\eta) \rightarrow 0 & \text{as } \eta = \infty \end{cases} \quad (3.10)$$

Step 2: Equation (3.2 - 3.9) is modified by adding the embedded factor p :

$$2\zeta_1 + \zeta_6 = 0, \quad (3.11)$$

$$2\zeta_2 + (S\frac{\eta+1}{2} - \zeta_5 f)(\zeta_2 - 1)p - \zeta_1^2 + \zeta_3^2 + S\zeta_1 = 0, \quad (3.12)$$

$$\zeta_4 + (S\frac{\eta+1}{2} - \zeta_5)(\zeta_4 - 1)p - 2\zeta_1\zeta_3 + S\zeta_3 = 0, \quad (3.13)$$

$$\zeta'_6 - (\zeta_5 - S\frac{\eta+1}{2})(\zeta_6 - 1)p + \frac{S\zeta_5}{2} = 0, \quad (3.14)$$

$$\zeta'_8 + (PrS(\frac{\eta+1}{2}) - Pr\zeta_5)(\zeta_8 - 1)p + PrDu\zeta'_{10} = 0, \quad (3.15)$$

$$\zeta'_{10} - (Sch - ScS(\frac{\eta+1}{2}))(\zeta_{10} - 1)p + ScSr\zeta'_8 = 0, \quad (3.16)$$

$$\zeta_{13} - Bt((S\frac{\eta}{2} - \zeta_5)(\zeta_{13} - 1)p + \zeta_{12}\zeta_6 + \zeta_1\zeta_6 + \zeta_5\zeta_2 + S\zeta_{12}) = 0, \quad (3.17)$$

$$\zeta'_{15} + Bt(2\zeta_5\zeta_{12} + 2\zeta_{14}\zeta_1 - \frac{S}{2}(\zeta_{15} - 1)p\eta + \zeta_{14}) = 0, \quad (3.18)$$

Step 3: Differentiating by parameter p

While differentiating Eqs. (3.11 - 3.18) for parameter p , come at the following system in terms of parameter p :

$$V' = AV + R, \quad (3.19)$$

where R and A is the remainder and coefficient matrix respectively.

$$V = \frac{d\zeta_i}{d\tau}, \quad i = 1, 2, \dots, 11 \quad (3.20)$$

Step 4: Use the superposition approach to each problem and characterize the Cauchy problem

$$V = aU + W \quad (3.21)$$

For each element, resolve the two Cauchy problems listed below.

$$U' = aU, \quad (3.22)$$

$$W' = AW + R \quad (3.23)$$

We get the approximate answer eq. (3.21) by plugging it into the original eq. (3.19).

$$(aU + W)' = A(aU + W) + R \quad (3.24)$$

Step 5: Solving the Cauchy problems

This study employs a numerical implicit methodology, which is detailed below.

$$\frac{U^{i+1} - U^i}{\Delta\eta} = AU^{i+1}, \quad \text{or } U^{i+1}(I - \Delta\eta A) = U^i, \quad (3.25)$$

$$\frac{W^{i+1} - W^i}{\Delta\eta} = AW^{i+1}, \quad \text{or } W^{i+1}(I - \Delta\eta A) = W^i \quad (3.26)$$

we get the iterative form of the solution.

$$U^{i+1} = (I - \Delta\eta A)^{-1}U^i, \quad (3.27)$$

$$W^{i+1} = (I - \Delta\eta A)^{-1}(W^i + \Delta\eta R), \quad (3.28)$$

4. Result and Discussion

The time-dependent viscous fluid flow across a gyrating disk with upward and downward fluctuation has been studied via using a parametric approach. The results have been reported through Figures and Tables.

Radial velocity profile:

Figure 2(a)-(d) elaborated the radial velocity profile versus contracting/ expanding term S , rotation parameter Γ , injection parameter β , and suction parameter $-\beta$ respectively. The radial velocity $f(\eta)$ is reduced with the contracting and relaxation S of the disk surface because the fluctuation of the surface opposes the flow particles as shown in Figure 2(a). The improvement in disk rotation Γ encourages the fluid particles and increases their kinetic energy as a result the radial velocity improves as elaborated through Figure 2(b). Figure 2(c) and (d) expressed that the radial velocity $f(\eta)$ enhances with the injection β effect and reduces with the impact of suction $-\beta$ force respectively. The injection effect added with fluid flow enhances the radial velocity, while the suction effect opposes the fluid velocity.

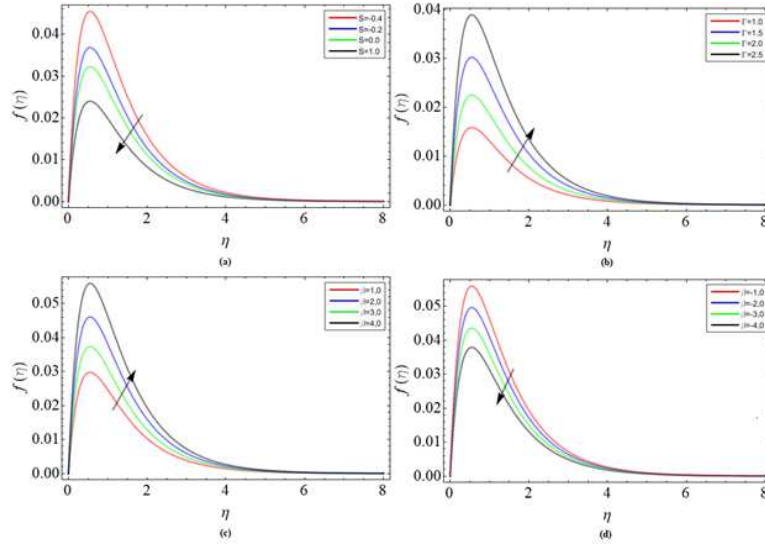


Figure 2: Radial velocity profile $f(\eta)$ versus (a) contracting/ expanding term S (b) rotation parameter Γ (c) injection paramter β (d) suction parameter $-\beta$

Azimuthal velocity profile:

Figure 3(a)-(d) revealed the same behavior as Figure 2(a)-(d) versus contracting/ expanding term S , rotation parameter Γ , injection parameter β , and suction parameter $-\beta$ respectively. The azimuthal velocity $g(\eta)$ is reduced with the contracting and relaxation S of the disk surface because the fluctuation of the surface opposes the flow particles as shown in Figure 3(a). The improvement in disk rotation Γ encourages the fluid particles and increases their kinetic energy as a result the azimuthal velocity improves as elaborated through Figure 3(b). Figure 3(c) and (d) expressed that the azimuthal velocity $g(\eta)$ enhances with the injection β effect and reduces with the impact of suction $-\beta$ force respectively. The injection effect added with fluid flow enhances the radial velocity, while the suction effect opposes the fluid velocity.

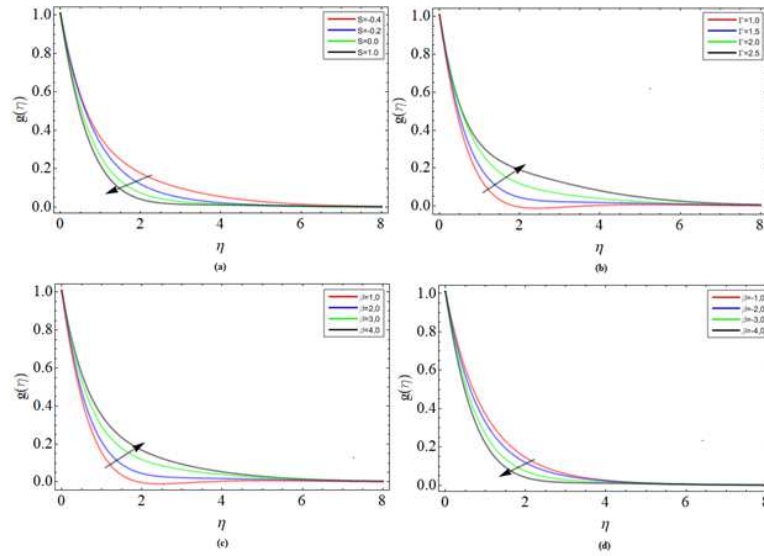


Figure 3: Azimuthal velocity profile $g(\eta)$ versus (a) contracting/ expanding term S (b) rotation parameter Γ (c) injection parameter β (d) suction parameter $-\beta$

Temperature profile:

Figure 4(a)-(c) illustrated the behavior of energy profile $\theta(\eta)$ versus Dufour number Du , heat transference Biot number β_1 , and Prandtl number Pr respectively. Figure 4(a) and (b) improves the fluid thermal energy profile against the Dufour number Du and heat transition Biot number β_1 profile. Physically, the kinetic viscosity and specific heat capacity of the fluid reduces with the increment of the Dufour number, as a result, the fluid thermal energy $\theta(\eta)$ profile enhances. Figure 4(c) demonstrated the reducing trend of temperature distribution versus Prandtl number. The specific heat capability and viscosity of fluid increase with the action of Prandtl number, as a result, the thermal profile rises.

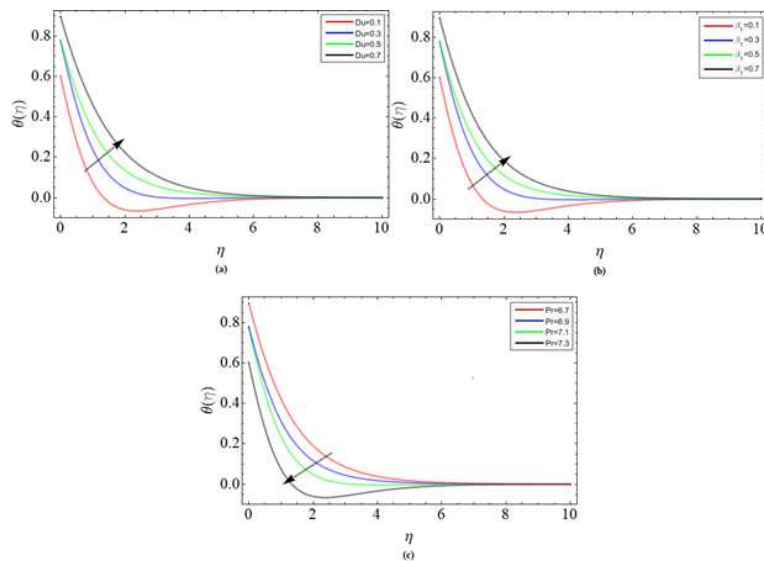


Figure 4: Temperature profile $\theta(\eta)$ versus (a) Dufour number Du (b) heat transfer Biot number β_1 (c) Prandtl number Pr

Concentration profile:

Figure 5(a)-(c) communicated the nature of energy profile $\varphi(\eta)$ versus Schmidt number Sc , Soret number Sr and mass transfer Biot number β_2 respectively. Figure 5(a) and (b) manifested that the mass transition rate declines with the action of Schmidt Sc and Soret number Sr . Because, the kinetic viscosity of fluid increases with the effect of Schmidt number, as a result, mass propagation rate declines as exhibited in Figure 5(a). The mass diffusivity rises with the increment of the Soret number, which causes the declination in the mass transition profile $\varphi(\eta)$ as appeared in Figure 5(b). On the other hand, mass propogation profile improves with the consequences of mass transfer Biot number β_2 . The mass diffusivity negatively effect with the mass transfer Biot number 2, which results in the elevation of mass propogation.

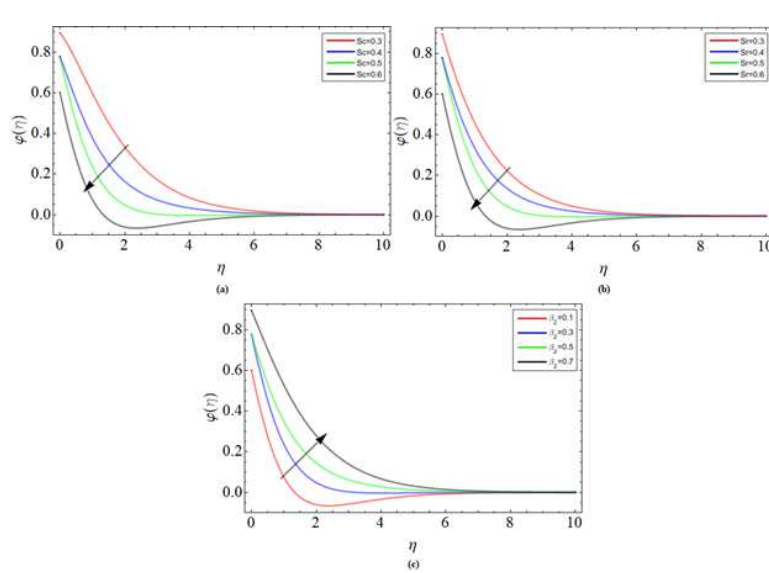


Figure 5: Concentration profile $\varphi(\eta)$ versus (a) Schmithd number Sc (b) Soret number Sr (c) mass transfer Biot number β_2

Magnetic strength profile:

Figure 6(a)-(d) revealed the nature of magnetic strength profile along radial $m'(\eta)$ and azimuthal $n(\eta)$ directions respectively. Figure 6(a) and (b) convey that the magnetic strength profile along radial $m'(\eta)$ direction versus the action of Batchlor number Bt enhances, while it reduces under the consequences of Reynold number Re . The same phenomena has been observed in the azimuthal direction $n(\eta)$ with against same paramters.

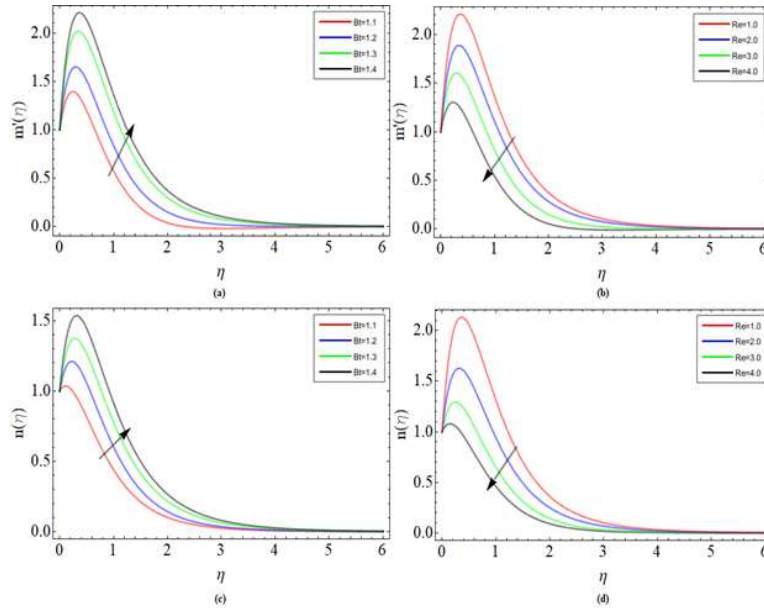


Figure 6: Radial $m'(\eta)$ and azimuthal $n(\eta)$ magnetic strength profile versus Batchlor Bt and Reynold number Re

Table 1 elaborates the comparative analysis between the existing literature with the present work for skin friction $f'(0)$ and $-g'(0)$. For reliability and validity of the proposed method Table 2 is plotted.

Table 1: The comparative analysis of the outcomes with the published work for skin friction $f'(0)$ and $-g'(0)$

S	β	β	Γ	[18] $f'(0)$	Present Work $f'(0)$	[18] $-g'(0)$	Present Work $-g'(0)$
-0.4				0.40732	0.40743	0.75172	0.75441
-0.2				0.44526	0.44612	0.68398	0.68476
0.0				0.48559	0.48876	0.161561	0.16321
1.0				0.58945	0.58987	0.44047	0.44153
	1.1			0.69276	0.69367	0.25762	0.25981
	2.0			0.54880	0.54912	0.50527	0.50712
	3.0			0.55748	0.55834	0.45456	0.45490
	4.0			0.56323	0.56452	0.40264	0.40312
	5.0			0.56351	0.56564	0.31115	0.32243
		0.0		0.53352	0.53382	0.57298	0.59321
		-1		0.51515	0.51545	0.64065	0.67072
		-2		0.49271	0.49342	0.071498	0.72578
		-3		0.46663	0.46677	0.79640	0.81432
		-4		0.43766	0.43321	0.88576	0.99567
			1.0	0.54763	0.54799	0.51115	0.61123
			1.5	0.95780	0.95998	1.00518	1.23211
			2.0	1.43242	1.43773	1.59766	1.98230
			2.5	1.96157	1.96287	2.27419	2.36711
			3.0	2.53845	2.53782	3.02524	3.43212

Table 2: The comparative analysis between PCM and bvp4c for $-\theta'(0)$

		PCM	bvp4c
Pr	Du	$-\theta'(0)$	$-\theta'(0)$
6.7		0.11954	0.11944
6.9		0.12824	0.12813
7.1		0.13646	0.13635
7.3		0.14856	0.14600
	0.3	0.15260	0.15120
	0.4	0.14458	0.14321
	0.5	0.13271	0.13173
	0.6	0.12732	0.11012

5. Conclusion

In this work, we examined the time-dependent viscous fluid flow over a rotating disk with upward and downward movement. The major goal of this research is to assess fluid flow under the influence of magnetic fields and heat propagation processes. The results have been found out through numerical procedure Parametric Continuation Method (PCM). For the scale reliability purpose, the outcomes are compared to another numerical Matlab scheme boundary value solver. The following conclusion have been made:

- 1) The radial velocity $f(\eta)$ is reduced with the contracting and relaxation S of the disk surface because the fluctuation of the surface opposes the flow. While, the improvement in disk rotation Γ encourages the fluid particles and increases their kinetic energy as a result the radial velocity improves.
- 2) The fluid thermal energy profile $\theta(\eta)$ improves against the variation in Dufour number Du and heat transition Biot number β_1 profile.
- 3) The dynamic viscosity and specific heat capacity of fluid increases with the action of Prandtl number, as a result, the thermal energy profile $f(\eta)$ rises.
- 4) The mass transition rate declines with the action of Schmidt Sc and Soret number Sr . Because, the kinetic viscosity of fluid increases with the effect of Schmidt number, as a result, mass propagation rate declines.
- 5) The magnetic strength profile along radial $m'(\eta)$ direction versus the action of Batchlor number Bt enhances, while it reduces under the consequences of Reynold number Re .

References

1. Lv Y.P., Algehyne E. A., Alshehri M.G., Alzahrani E., Bilal, M. Khan, M.A. and Shuaib, M., *Numerical approach towards gyrotactic microorganisms hybrid nanoliquid flow with the hall current and magnetic field over a spinning disk*, Scientific Reports, 11(1), 1-13, (2021).
2. Hafeez A., Khan M. and Ahmed J., *Thermal aspects of chemically reactive Oldroyd-B fluid flow over a rotating disk with Cattaneo-Christov heat flux theory*, Journal of Thermal Analysis and Calorimetry, 144(3), 793-803, (2021).
3. Ahmadian A., Bilal M., Khan M.A. and Asjad, M.I., *Numerical analysis of thermal conductive hybrid nanofluid flow over the surface of a wavy spinning disk*, Scientific reports, 10(1), 1-13, (2020).
4. Khan M.I., *Transportation of hybrid nanoparticles in forced convective Darcy-Forchheimer flow by a rotating disk*, International Communications in Heat and Mass Transfer, 122, 105177, (2021).
5. Li Y.X., Muhammad T., Bilal M., Khan M.A., Ahmadian A. and Pansera, B.A., *Fractional simulation for Darcy-Forchheimer hybrid nanoliquid flow with partial slip over a spinning disk*, Alexandria Engineering Journal, 60(5), 4787-4796, (2021).
6. Zhou S.S., Bilal M., Khan M.A. and Muhammad, T., *Numerical Analysis of Thermal Radiative Maxwell Nanofluid Flow Over-Stretching Porous Rotating Disk*, Micromachines, 12(5), <https://doi.org/10.3390/mi12050540>, (2021).
7. Tassaddiq A., Khan S., Bilal M., Gul T., Mukhtar S., Shah Z. and Bonyah E., *Heat and mass transfer together with hybrid nanofluid flow over a rotating disk*, AIP Advances, 10(5), 055317, (2020).
8. Marmanis H., *Analogy between the Navier-Stokes equations and Maxwell's equations: application to turbulence*, Physics of fluids, 10(6), 1428-1437, (1998).
9. Kambe T., *A new formulation of equations of compressible fluids by analogy with Maxwell's equations*, Fluid dynamics research, 42(5), 055502, (2010).

10. Luo F., Yao H. and Zhu C., *Stability of rarefaction wave for isentropic compressible Navier–Stokes–Maxwell equations*, *Nonlinear Analysis: Real World Applications*, 59, 103234, (2021).
11. Yao H., Yin H. and Zhu C., *Stability of rarefaction wave for the compressible non-isentropic Navier–Stokes–Maxwell equations*, *Communications on Pure and Applied Analysis*, 20(3), 1297, (2021).
12. Ahmadian A., Bilal M., Khan M.A. and Asjad M.I., *The non-Newtonian maxwell nanofluid flow between two parallel rotating disks under the effects of magnetic field*, *Scientific Reports*, 10(1), 1-14, (2020).
13. Zhang Z., *A convergence to the Navier–Stokes–Maxwell system with solenoidal Ohm’s law from a two-fluid model*, *Proceedings of the Royal Society of Edinburgh Section A: Mathematics*, 151(3), 1094-1115, (2021).
14. Patil A., *A Modification and Application of Parametric Continuation Method to Variety of Nonlinear Boundary Value Problems in Applied Mechanics*, Thesis, (2016).
15. Shuaib M., Shah R.A. and Bilal M., *Variable thickness flow over a rotating disk under the influence of variable magnetic field: An application to parametric continuation method*, *Advances in Mechanical Engineering*, 12, 1687814020936385, (2020).
16. Shuaib M., Shah R.A., Durrani I. and Bilal M., *Electrokinetic viscous rotating disk flow of Poisson–Nernst–Planck equation for ion transport*, *Journal of Molecular Liquids*, 313, 113412, (2020).
17. Dombovari Z., Iglesias A., Molnar T.G., Habib G., Munoa, Kuske, R. and Stepan G., *Experimental observations on unsafe zones in milling processes*, *Philosophical Transactions of the Royal Society A*, 377, 20180125, (2019).
18. Shehzad S.A., Abbas Z., Rauf A. and Abdelmalek Z., *Dynamics of fluid flow through Soret–Dufour impacts subject to upward and downward motion of rotating disk*, *International Communications in Heat and Mass Transfer*, 120, 105025, (2021).
19. Ali S., Khan A., Shah K., Alqudah M.A, Abdeljawad T. and Islam S., *On computational analysis of highly nonlinear model addressing real world applications*, *Results in Physics*, 36, 105431, (2022).
20. Shah K., Naz H., Sarwar M. and Abdeljawad T., *On spectral numerical method for variable-order partial differential equations*, *AIMS Mathematics*, 7(6), 10422-10438, (2022).

Samia Bushnaq,
Department of Basic Sciences,
King Abdullah II of Engineering, Princess Sumaya University for Technology,
Jordan.
E-mail address: s.bushnaq@psut.edu.jo

and

Asif Ullah Hayat,
Department of Mathematics,
Abdul Wali Khan University, 23200 Mardan,
Pakistan.
E-mail address: asifhayat767@gmail.com

and

Hassan Khan,
Department of Mathematics,
Abdul Wali Khan University, 23200 Mardan,
Pakistan.
E-mail address: hassanmath@awkum.edu.pk